Efficient Finite Element and Contact Procedures for the Simulation of High Speed Sheet Metal Forming Processes*

M. Schwarze[1], A. Brosius[2], S. Reese[1], M. Kleiner[2]

[1]Institute of Solid Mechanics, University Carolo-Wilhelmina at Braunschweig, Germany
[2]Institute of Forming Technology and Lightweight Construction, University of Dortmund, Germany

Abstract

A large variety of forming processes is used in industrial manufacturing processes. The numerical simulation of such processes puts high demands on the finite element technology. Usually first order isoparametric elements are preferred because of their robustness and numerical efficiency. Unfortunately, these elements tend to undesired numerical effects like "locking", predominant in situations characterized by plastic incompressibility or pure bending. To overcome this problem, several authors [1, 2, 4] propose finite element formulations based on the concept of reduced integration with hourglass stabilization by applying the "enhanced strain method". The main advantage of the proposed new isoparametric solid-shell formulation with linear ansatz functions is the fact that the undesirable effects of locking are eliminated.
The previously described element technique can be applied to analyze specific problems of high speed forming into a cavity: Working with contact surfaces discretized by first order finite elements leads to discontinuities of the normal patch vector and, subsequently, to non-smooth sliding [5]. In quasi-static forming processes these discontinuities will not influence the contact forces noticeably. However, in dynamic investigations the sudden change of contact forces due to the rough surface description leads to a very high acceleration of the contact nodes. To avoid this effect, a smoothing algorithm will be described.

Keywords:

Sheet metal forming, Solid-shell formulation, Contact formulation

*This work is based on the results of the research group FOR 443. The authors wish to thank the German Research Foundation – DFG for its financial support.

1 Introduction

In mechanical engineering, e.g. in car industries, the development and optimization of forming tools and their parameters according to the desired forming result is a cost and time intensive factor of the production process. In order to reduce expensive try-out processes, numerical tools, especially the finite element method, are applied before setting up the forming tools. The numerical simulation of forming processes makes high demands on the finite element technology. Finite element formulations with low order ansatz functions are preferred due to their numerical efficiency and robustness. Furthermore, they prove to be advantageous when automatic meshing tools are applied.

During the forming process the structure underlies extreme bending. Furthermore, the material shows nearly incompressible behavior during plastification. By using the standard finite element formulation with linear ansatz functions (Q1) the undesirable effect of locking can be observed. It leads to an overestimation of the stresses and an underestimation of the deformation. One possibility to overcome locking is the use of element formulations with high ansatz order. However, then one can not profit from the advantages described before. In the field of element technology modifications of classical low order finite element formulations are derived to avoid the non-physical effect of locking. A possible strategy is the method of incompatible modes. It is the basis of the enhanced assumed strain (EAS) concept [16]. Based on a mixed variational principle additional ”enhanced” strains are introduced to avoid the non-physical constraint caused by the low order ansatz functions. In problems under compression numerical instabilities might arise [17]. A second concept in finite element technology is the method of reduced integration. The integration over a smaller number of integration points eventually leads to non-physical zero-modes (hourglassing). For this reason an hourglass stabilization is necessary. Several authors (e.g. [17, 1, 18] and [4]) have worked on reduced integration with hourglass stabilization in combination with the EAS concept. The results are simple, robust, and efficient element formulations. For the special context of sheet metal forming processes a so-called solid-shell formulation with reduced integration and hourglass stabilization by means of the EAS concept is derived. It only has displacement degrees-of-freedom and takes the element thickness correctly into account.

In forming processes contact between work tools and workpiece occur. The treatment of contact problems is an important aspect in the finite element analysis of forming processes. In the context of the computational modeling we differentiate between deformable-to-deformable contact (including self contact) and deformable-to-rigid contact. In the first case the description of all contact surfaces depends on the discretized domain. Due to the use of modern and efficient element formulations only a relative coarse mesh is necessary. By using finite element formulations with linear ansatz functions contact surfaces are modeled as being piecewise linear. This leads to a non-smooth normal patch vector and to non-smooth sliding. We observe sudden changes of contact forces and jumps in the velocity field. Furthermore, using an implicit time integration a divergence of the Newton-Raphson scheme and numerical instabilities might arise.

To avoid these non-physical effects, various approaches to smoothen the contact surface are developed. For two-dimensional cases in [5, 8] the interpolation polynomials are defined at the midpoints of neighbored element edges, whereas in [7, 9] the element nodes themselves are

used. In the first case the contact interface lies inside the discretized domain and in the second case it is modeled at the outside. Three-dimensional smoothing procedures are formulated by [10, 12].
The contact formulation presented here follows geometrically the smoothing strategy of [5] for the two-dimensional case. The contact interpolation is carried out by cubic Hermite ansatz functions. The new aspect in this approach is the smoothing of slave surface and master surface as well. This leads to a quasi-segment-to-segment approach with six nodes per contact element (three for the slave segment and three for the master segment). The contact interface can be correctly taken into account by using a gauss integration over the slave surface.

2 Solid-shell formulation

The basic equation set of continuum mechanics will be given here for the dynamic case without damping

$$Div\,\mathbf{P} + \rho_0\,(\mathbf{b}_v - \ddot{\mathbf{u}}) = \mathbf{0} \tag{1}$$

$$\mathbf{P} - \frac{\partial W}{\partial \mathbf{H}} = \mathbf{0} \tag{2}$$

$$\mathbf{H} - Grad\,\mathbf{u} = \mathbf{H}_{enh} = \mathbf{0} \tag{3}$$

Equation 1 denotes the balance of linear momentum, in which ρ_0 is the reference mass density and $\rho_0\mathbf{b}_v$ the vector of volume forces, e.g. the gravity. In the constitutive equation (Equation 2) $W = W(\mathbf{H}, \mathbf{X})$ defines the strain energy function as a function of the total strain $\mathbf{H}$ and the vector of internal variables $\mathbf{X}$. $\mathbf{P}^h$ is the first Piola-Kirchhoff stress tensor. The total strain $\mathbf{H}$ is additively decomposed into the compatible strain $Grad\,\mathbf{u}$ and the enhanced part $\mathbf{H}_{enh}$, compare Equation 3. The index h denotes the finite element discretization of the domain. Starting point of the solid-shell formulation is the two-field functional

$$g_1(\mathbf{u}^h, \mathbf{H}^h_{enh}) = \int_{B_0^h} \tilde{\mathbf{P}}(\mathbf{H}^h) : Grad\,\delta\mathbf{u}^h\,dV + \int_{B_0^h} \rho_0\,\ddot{\mathbf{u}}\,\delta\mathbf{u}^h\,dV - g_{ext} = 0 \tag{4}$$

$$g_2(\mathbf{u}^h, \mathbf{H}^h_{enh}) = \int_{B_0^h} \tilde{\mathbf{P}}(\mathbf{H}^h) : \delta\,\mathbf{H}^h_{enh}\,dV = 0 \tag{5}$$

in which the displacement vector $\mathbf{u}^h$ and the tensor of enhanced strains $\mathbf{H}^h_{enh}$ are the independent variables. The term g_{ext} includes the virtual work of the external forces. In the following all values are given in matrix notation. The interpolation of $\mathbf{H}^h$ does not differ from the one chosen for the hexahedral element formulation proposed by [14]:

$$\mathbf{H}^h = \underbrace{(\mathbf{B}_{lin} + (\mathbf{j}_0^1\,\mathbf{L}^1_{hg} + \mathbf{j}_0^2\,\mathbf{L}^2_{hg})\,\mathbf{M}_{hg})\,\mathbf{U}_e}_{:=\mathbf{H}^h_{comp}=\mathbf{H}^h_{lin}+\mathbf{H}^h_{hg}} + \underbrace{\mathbf{j}_0^1\,\mathbf{L}^1_{enh}\,\mathbf{W}_e}_{:=\mathbf{H}^h_{enh}} \tag{6}$$

It is well known that the hourglass part $\mathbf{H}^h_{hg}$ of the compatible strain tensor $\mathbf{H}^h_{comp}$ includes the locking behavior, whereas the linear part $\mathbf{H}^h_{lin}$ does not include any constraints which lead to locking. For the definition of variables used above, see [3]. In contrast to classical finite element formulations the Jacobian matrix is always evaluated in the center of the element. Further modifications avoid volumetric locking [15].

At the present point of the derivation the formulation does not differ majorly from [15]. However, the analysis of thin structures with only one element over the thickness is the main target of the development of the formulation from the numerical point of view. So the main question is how to transfer the three-dimensional formulation into a solid-shell concept. A good description of the stress state over the thickness is very important. The first Piola-Kirchhoff stress tensor has to be non-linear in thickness direction. For this reason a Taylor expansion is carried out with respect to the point $\boldsymbol{\xi}_\star^T = \{0, 0, \xi\}$, see Figure 1. In this way the non-linear dependence on ζ is retained in the constitutive qualities, namely the stress $\mathbf{P}_\star^h$ and the tangent $\mathbf{A}_\star$. This leads to the split

$$\mathbf{P}^h \approx \mathbf{P}^h\Big|_{\boldsymbol{\xi}=\boldsymbol{\xi}_\star} + \frac{\partial \mathbf{P}^h}{\partial \xi}\Big|_{\boldsymbol{\xi}=\boldsymbol{\xi}_\star} (\xi - 0) + \frac{\partial \mathbf{P}^h}{\partial \eta}\Big|_{\boldsymbol{\xi}=\boldsymbol{\xi}_\star} (\eta - 0) \tag{7}$$

$$= \mathbf{P}_\star^h + \mathbf{A}_\star^h \left(\left(\mathbf{j}_0^1 \, \mathbf{L}_{hg\star}^1 + \mathbf{j}_0^2 \, \mathbf{L}_{hg\star}^2 \right) \mathbf{M}_{hg} \, \mathbf{U}_e + \mathbf{j}_0^1 \, \mathbf{L}_{enh\star} \, \mathbf{W}_e \right) \tag{8}$$

of the stress tensor. $\mathbf{P}_\star^h$ is non-linear in the thickness direction ζ and independent of ξ and η.

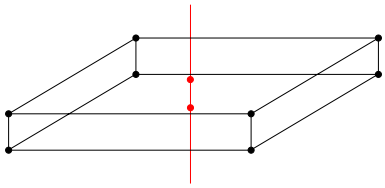

Figure 1: Solid-shell element

The second term is non-linear in ζ and linear in ξ and η. The stresses are therefore non-linear in thickness direction and linear in the shell plane. $\mathbf{A}_\star^h$ denotes the derivative of $\tilde{\mathbf{P}}(\mathbf{H}^h)$ with respect to the total strain $\mathbf{H}^h$ (consistent tangent). At the element level the following steps are executed: The identification of the thickness direction will be performed by a coordinate transformation. Furthermore, the analysis of the enhanced degrees-of-freedom is necessary. Using Equation 8, they are determined by the non-linear equation

$$\mathbf{R}_w = \int_{\zeta=-1}^{\zeta=+1} \hat{\mathbf{L}}^{\zeta T} \, \mathbf{j}_0^{1T} \, \mathbf{P}_\star^h \, d\zeta \, 4J_0 \tag{9}$$

for $\mathbf{W}_e^\zeta$ and the linear equation

$$\mathbf{W}_e^{\xi\eta} = -\mathbf{K}_{ww} \, \mathbf{K}_{wu} \, \mathbf{U}_e \tag{10}$$

for $\mathbf{W}_e^{\xi\eta}$. Due to the linearity of Equation 10 only a reduced number of enhanced degrees-of-freedom, namely the three values $\mathbf{W}_e^\zeta$, have to be saved as history variables.
The differential equation

$$\mathbf{R}_{uG}(\mathbf{U}) + \mathbf{K}_{stab,G} \, \mathbf{U} + \mathbf{M}_G \, \ddot{\mathbf{U}} - \mathbf{F}_{ext} = \mathbf{0} \tag{11}$$

which finally results from the weak form, has to be analyzed in every time step. In comparison to the classical form, the product of the stabilization matrix $\mathbf{K}_{stab,G}$ and the global displacement vector $\mathbf{U}$ is added. The element stabilization matrix $\mathbf{K}_{stab,e}$ has the form

$$\mathbf{K}_{stab,e} = \int_\square \mathbf{B}_{def}^T \mathbf{A}_\star \mathbf{B}_{def} \, d\xi \, d\eta \tag{12}$$

In the context of implicit time integration Equation 11 is usually solved by means of the Newton-Raphson iterative algorithm. This makes it necessary to compute the derivative of $\mathbf{A}_\star$ with respect to the deformation. In order to avoid this elaborate task, we replace $\mathbf{A}_\star$ by an artificial stiffness $\mathbf{A}_{\star,art}$ with the form

$$\mathbf{A}_{\star,art} = \mu_\star \begin{pmatrix} \bullet & & & & & & & & & & & \\ & \bullet & & & & & & & & & & \\ & & \bullet & & & & & & & & & \\ & & & \bullet & \bullet & & & & & & & \\ & & & \bullet & \bullet & & & & & & & \\ & & & & & \bullet & \bullet & & & & & \\ & & & & & \bullet & \bullet & & & & & \\ & & & & & & & \bullet & \bullet & & & \\ & & & & & & & \bullet & \bullet & & & \\ & & & & & & & & & \bullet & \bullet & \\ & & & & & & & & & \bullet & \bullet & \end{pmatrix} \tag{13}$$

is used. It basically depends on the coefficient $\mu_\star$. Its lower border is given by

$$\mu_\star = \mu\tilde{H}/(\tilde{H} + E) \tag{14}$$

in which μ denotes the shear modulus, $\tilde{H}$ the hardening parameter at the beginning of plastification, and E the Young's modulus. To avoid the given estimation, we currently work on an adaptive computation depending on the degree of plastification.
The advantages of the given solid-shell formulation can be summarized as follows:

- In the element formulation given above the undesirable effect of locking is eliminated.
- The computational cost reduces noticeably: In sheet metal simulations the need of only one element over the thickness leads to a reduced number of elements. Due to the use of only two gauss points per element a smaller number of loops at the element level is necessary.
- In the case of electromagnetic forming a simplified search algorithm for the identification of the sheet metal in the discetized domain can be applied.
- The element formulation takes the sheet thickness correctly into account. This is advantageous for the use in contact simulations.

3 Two-dimensional C^1-continuous six-node contact element

The general framework of the continuum-based finite element formulation for large deformation contact can be found in [13]. We follow the classical master-slave technique and assume the contact of two bodies B^γ, with γ = 1 for the master-body and γ = 2 for the slave-body, see Figure 2. The constraint equations are formulated with respect to the deformed configuration. The reference state vector $\mathbf{X}^\gamma$ and the displacement vector $\mathbf{u}^\gamma$ lead to the current coordinates $\mathbf{x}^\gamma = \mathbf{X}^\gamma + \mathbf{u}^\gamma$. For every given slave point $\mathbf{x}^2$ on the slave surface ${\beta_c}^2$ a corresponding master

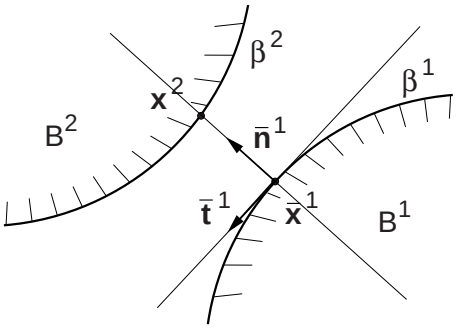

Figure 2: Contact kinematic

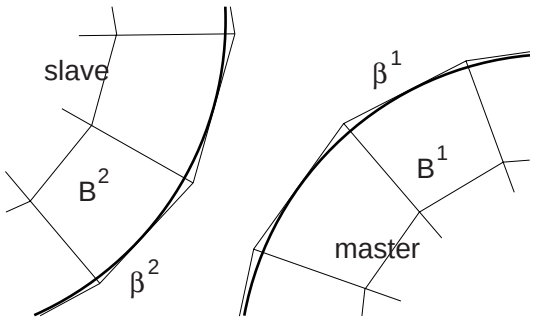

Figure 3: Smoothing concept

point $\bar{\mathbf{x}}^1$ on the master surface ${\beta_c}^1$ has to be found. Assuming a convex surface description of a two-dimensional problem, the minimum distance problem

$$|g_n| = \|\mathbf{x}^2 - \bar{\mathbf{x}}^1\| = min\|\mathbf{x}^2(\hat{\xi}) - \bar{\mathbf{x}}^1(\bar{\xi})\| \tag{15}$$

has to be investigated. $\mathbf{x}^2(\hat{\xi})$ denotes the current slave node depending on the gauss point coordinate $\hat{\xi}$ and $\bar{\mathbf{x}}^1(\bar{\xi})$ is the master node at the convective solution coordinate $\bar{\xi}$. The unit outward normal vector at the master surface can be defined as

$$\bar{\mathbf{n}}^1(\bar{\xi}) := \frac{\bar{\mathbf{t}}^1(\bar{\xi}) \times \mathbf{e}_3}{\|\bar{\mathbf{t}}^1(\bar{\xi}) \times \mathbf{e}_3\|} \tag{16}$$

in which the cartesian basis vector $\mathbf{e}_3$ indicates the outward normal vector on the sheet plane. The tangent vector is computed by

$$\bar{\mathbf{t}}^1(\bar{\xi}) = \frac{\partial \bar{\mathbf{x}}^1(\bar{\xi})}{\partial \xi} \, \| \frac{\partial \bar{\mathbf{x}}^1(\bar{\xi})}{\partial \xi} \|^{-1} \tag{17}$$

If non-linear contact surface descriptions are used, Equation 15 leads with

$$[\mathbf{x}^2(\hat{\xi}) - \bar{\mathbf{x}}^1(\bar{\xi})] \cdot \frac{\partial \bar{\mathbf{x}}^1(\bar{\xi})}{\partial \xi} = 0 \tag{18}$$

to a non-linear equation system. The gap function

$$g_n = [\mathbf{x}^2(\hat{\xi}) - \bar{\mathbf{x}}^1(\bar{\xi})] \cdot \bar{\mathbf{n}}^1(\bar{\xi}) \tag{19}$$

declares the contact condition between the slave and master node. If $g_n > 0$ no contact holds, for $g_n = 0$ perfect contact, and if $g_n < 0$ penetration occurs.

As depicted in Figure 3 we model the contact smoothing along the element edges in a similar way to [5] and [10]. The starting point $\mathbf{x}_a$ and the end point $\mathbf{x}_b$ of the contact segment are defined by

$$\mathbf{x}_i = \sum_{k=1}^{2} N_k(\phi_i) \, \mathbf{x}_k \,, \quad i = a, b \tag{20}$$

in which N_k ($k = 1, 2$) denote the classical linear ansatz functions, see Figure 4, and $\mathbf{x}_k$ the nodes of the adjacent element edge. ϕ_a and ϕ_b are user defined convective coordinates. Using a cubic Hermite interpolation, e.g. [11], the contact segment

$$\mathbf{x}(\xi) = H_1(\xi) \, \mathbf{x}_a + H_2(\xi) \, \mathbf{x}_b + H_3(\xi) \, \beta_a \, l_a \, \mathbf{t}_a + H_4(\xi) \, \beta_b \, l_b \, \mathbf{t}_b \tag{21}$$

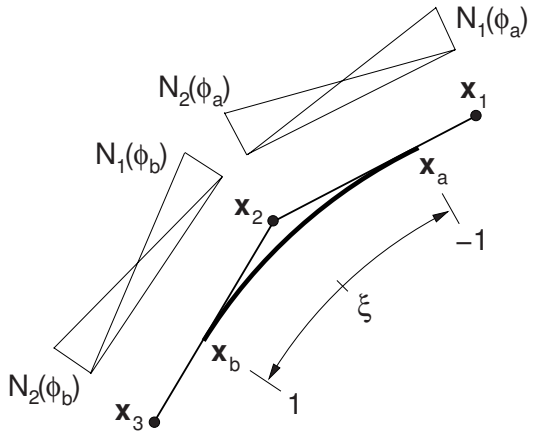

Figure 4: Contact segment definition

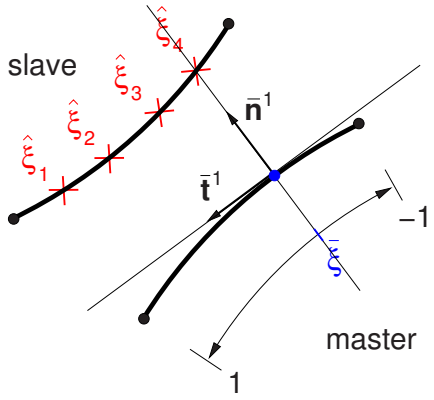

Figure 5: Gauss point integration

with the weighted tangents

$$l_a\,\mathbf{t}_a = \frac{1}{2}(\mathbf{x}_2 - \mathbf{x}_1) \quad and \quad l_b\,\mathbf{t}_b = \frac{1}{2}(\mathbf{x}_3 - \mathbf{x}_2) \tag{22}$$

at the starting point $\mathbf{x}_a$ and the end point $\mathbf{x}_b$ is defined by the Hermite functions

$$H_1(\xi) = \frac{1}{4}(2 - 3\,\xi + \xi^3), \quad H_3(\xi) = \frac{1}{4}(1 - \xi - \xi^2 + \xi^3),$$

$$H_2(\xi) = \frac{1}{4}(2 + 3\,\xi - \xi^3), \quad H_4(\xi) = \frac{1}{4}(-1 - \xi + \xi^2 + \xi^3), \tag{23}$$

the factors β_a and β_b and the element nodes $\mathbf{x}_1, \mathbf{x}_2$ and $\mathbf{x}_3$ of the discretized domain. For simplification reasons we define $\beta_a = \beta_b = \beta$. In contrast to other authors ([7], [9]) the slave contact surface as well as the master surface is smoothed, see Figures 3 and 5. This leads to a quasi-segment-to-segment approach discretized by a six-node contact element formulation. Using Equation 22 and 23, Equation 21 reduces after rearranging to

$$\mathbf{x}^2(\hat{\xi}) = \sum_{k=1}^{3} c_k(\hat{\xi})\,\mathbf{x}_k^2 \quad and \quad \bar{\mathbf{x}}^1(\bar{\xi}) = \sum_{k=1}^{3} c_k(\bar{\xi})\,\mathbf{x}_k^1 \tag{24}$$

for the current slave node $\mathbf{x}^2(\hat{\xi})$ at the gauss point $\hat{\xi}$ and its master node $\bar{\mathbf{x}}^1(\bar{\xi})$. The coefficients c_k ($k = 1, 2, 3$) include the Hermite ansatz functions as well as the definition of the starting point and the end point of the current segment. A gauss integration over the slave segment allocates the contact constraints over the contact element nodes. The path length between $\mathbf{x}_a^2$ and $\mathbf{x}_b^2$ is defined by

$$\int_{s_a^2}^{s_b^2} (\bullet)\, ds^2 \;=\; \int_{\hat{\xi}=-1}^{\hat{\xi}=1} (\bullet)\, detJ\, d\hat{\xi} \;\approx\; \sum_{k=1}^{n_g} (\bullet)|_{\hat{\xi}}\, w_k\, det\, J_k \tag{25}$$

in which w_k denotes the weighting factor and n_g the number of gauss points over the slave segment. The determinant of the Jacobian matrix

$$det\, J_k = \| \frac{\partial\, \mathbf{x}^2(\hat{\xi})}{\partial\, \hat{\xi}} \| \tag{26}$$

maps between the physical and the convective coordinates.
The classical weak form [13, 5] of the normal contact contributions for the penalty method

$$G_c = \int_{\beta^2} \epsilon_n \, g_n \, \delta g_n \, dA^2 = \int_{\beta^2} \epsilon_n \, g_n \, \overline{\mathbf{n}}^1(\bar{\xi}) \cdot [\delta \mathbf{u}^2 - \delta \overline{\mathbf{u}}^1(\bar{\xi})] \, dA^2 \tag{27}$$

depends on the penalty parameter ϵ_n for the normal contact, the gap function g_n and the variation of the displacement vectors $\delta \mathbf{u}^2$ and $\delta \overline{\mathbf{u}}^1(\bar{\xi})$. Discretizing the contact contribution given in Equation 28 by means of the smooth six-node contact element formulation described above leads to

$$G_c \approx \sum_{j=1}^{n_s} \sum_{k=1}^{n_g} \epsilon_n \, g_{n,k} \, \overline{\mathbf{n}}^1(\bar{\xi}_k) \cdot [\delta \mathbf{u}^2(\hat{\xi}_k) - \delta \overline{\mathbf{u}}^1(\bar{\xi}_k)] \, w_k \, det \, J_k \tag{28}$$

where $\hat{\xi}_k$ denotes the kth gauss point coordinate of the jth slave segment and $\bar{\xi}_k$ the convective solution coordinate at the contact segment to the given slave node. If contact occurs there exists only one master segment according the current slave node.
The advantages of the given two-dimensional smooth six-node contact element can be summarized as follows:

- The smooth contact surface description approximately re-establishes the natural surface of the bodies coming in contact. It leads to a smooth computation of the normal vector and works independently of the finite element formulation and its ansatz functions.
- In this way artificial jumps in the contact constraints over the iterations are avoided and, consequently, in the displacement field and its derivatives. A better convergence of the Newton-Raphson scheme can be achieved.
- Smoothing the slave surface as well as the master one leads to a quasi-segment-to-segment approach. A correct integration over the contact surface is possible.
- The given contact formulation allows the implementation of contact material laws at the slave surface.

4 Numerical examples

The numerical examples present simulations of an electromagnetic forming process. The geometry of the workpiece is depicted in Figure 6. The material parameters of the aluminum

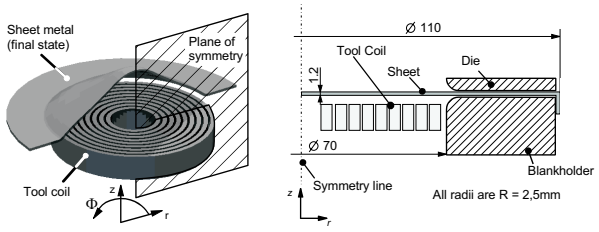

Figure 6: Workpiece, tool coil and die [21]

alloy AC 120 can be found in [19] and [20]. A viscoplastic material model based on a classical overstress formulation is used. To simulate electromagnetic forming, additional terms have to be considered in the balance equations. In the balance of linear momentum so-called Lorentz forces are introduced and in the balance of energy the electromotive power has to be considered. The additional unknown variables are the vector potential and the scalar potential.
In the first simulation we analyze the free forming process using the three-dimensional solid-shell formulation described above. The study of convergence in Figure 7 shows that already

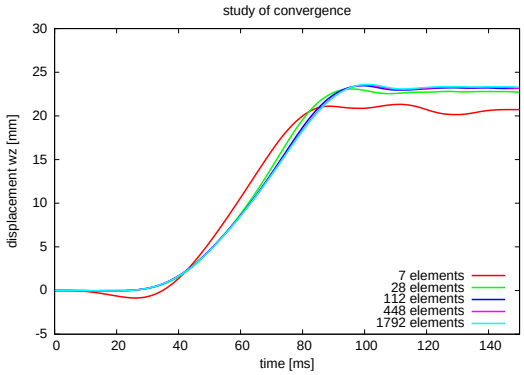

Figure 7: sheet midpoint displacement

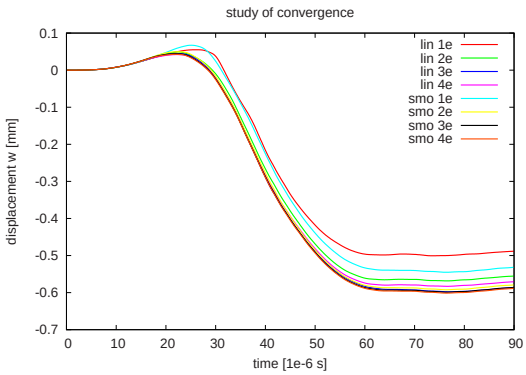

Figure 8: displacement node 81

a mesh with 112 elements (for the quarter structure) leads to a converged result. Depicted is the displacement of the sheet midpoint over time. At the beginning of the forming process the sheet metal is accelerated over the tool coil caused by the Lorentz forces. After that the work of deformation is done by the mass inertia (kinetic energy). In Figures 9 and 10 the Cauchy

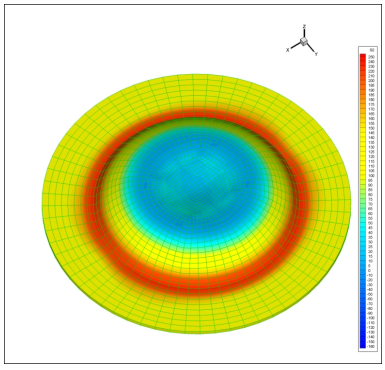

Figure 9: Cauchy stress at t = 55 μs

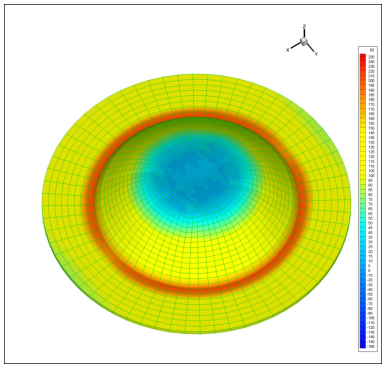

Figure 10: Cauchy stress at t = 70 μs

stresses at the times t = 55 μs and t = 70 μs are depicted.
The second simulation uses the same parameters given before. We compute the forming process by using the axissymmetric version of the solid-shell concept. The die restricts the forming geometry by an angle of 35.7 degrees. It is approximated as a rigid surface. We compare a piecewise linear contact description (see Figure 11) and a formulation using cubic Hermite ansatz functions (Figure 12) to discretize a radius of 5 mm of the die. In Figure 13 and 14 different states of deformation are depicted. A study of convergence for the horizontal

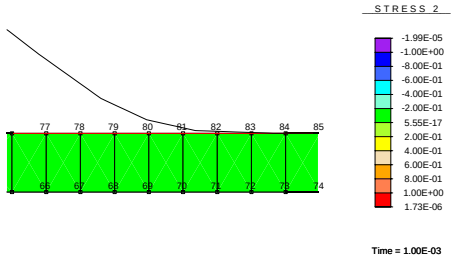

Figure 11: Piecewise linear contact

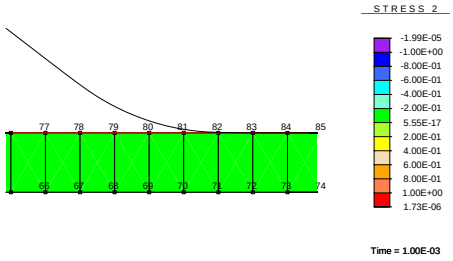

Figure 12: Smooth contact

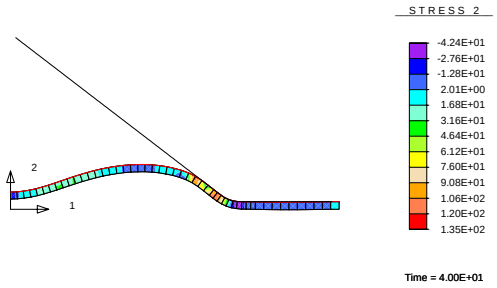

Figure 13: Deformation at t = 40 μs

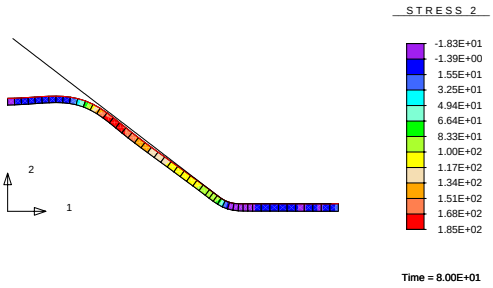

Figure 14: Deformation at t = 80 μs

displacement of node 81 is given in Figure 8. We start discretizing the radius with one contact segment (lin1e and smo1e). Already two smooth contact segments are necessary to achieve a nearly converged result. In comparison to this using the linear discretizing four segments are necessary. Furthermore, the usage of the Hermite contact formulation leads to a better convergence behavior of the Newton-Raphson scheme during the implicit time integration.

5 Conclusion and Outlook

In the present paper two aspects of modeling high speed forming processes by means of the finite element method are described. The first one enfolds the formulation of a solid-shell element using a reduced integration schema and a physically oriented stabilization technique. The second aspect deals with a smooth contact formulation suitable for modeling impact processes present at the electromagnetic forming. The element as well as the contact formulation was successfully implemented into a commercial finite element code in order to demonstrate the capability as well as the convergence behavior separately. Future work will be done to combine both beneficial developments into one code in order to simulate the high speed forming process of electromagnetic forming in a time-efficient, robust way without looking effects and numerical oscillations due to contact condition.

References

[1] *T. Belytschko & L. P. Bindemann.* Assumed strain stabilization of the eight node hexahedral element. *Computer Methods in Applied Mechanics and Engineering*, 105: 225–260, 1993.

[2] *R. Hauptmann, K. Schweizerhof & S. Doll.* Extension of the 'solid-shell' concept for application to large elastic and large elastoplastic deformations. *International Journal for Numerical Methods in Engineering*, 49:1121–1141, 2000.

[3] *S. Reese.* On a physically stabilized one point finite element formulation for three-dimensional finite elasto-plasticity. *Computer Methods in Applied Mechanics and Engineering*, 194: 4685–4715, 2005.

[4] *S. Reese.* A large deformation solid-shell concept based on reduced integration. *International Journal for Numerical Methods in Engineering*, submitted.

[5] *P. Wriggers, L. Krstulovic-Opara & J. Korelc.* Smooth C^1-interpolations for two-dimensional frictional contact problems. *International Journal for Numerical Methods in Engineering*, 51:1469–1495, 2001.

[6] *D. Risch, C. Beerwald, A. Brosius & M. Kleiner.* On the Significance of the Die Design for Electromagnetic Sheet Metal Forming. *Proc. of the ICHSF 2004 - 1st Int. Conference on High Speed Forming, 31.3.-1.4.2004, Dortmund*, 191–200, ISBN 3-00-012970-7.

[7] *N. El-Abbasi, S. A. Meguid & A. Czekanski.* On the modelling of smooth contact surfaces using cubic splines. *International Journal for Numerical Methods in Engineering*, 50:953–967, 2001.

[8] *L. Krstulovic-Opara & P. Wriggers.* A two-dimensional C^1-continuous contact element based on the moving friction cone decription. *Fifth World Congress on Computational Mechanics, July 7-12, Vienna, Austria*.

[9] *M. Stadler, G.A. Holzapfel & J.Korelc.* C^n continuous modelling of smooth contact surfaces using NURBS and application to 2D problems. *International Journal for Numerical Methods in Engineering*, 57:2177–2203, 2003.

[10] *L. Krstulovic-Opara, P. Wriggers & J.Korelc.* A C^1-continuous formulation for 3D finite deformation frictional contact. *Computational Mechanics*, 29: 27–42, 2002.

[11] *G. Dhatt, G. Touzot & G. Cantin.* The Finite Element Method Displayed. *John Wiley & Sons*, 1984.

[12] *M. A. Puso & T. A. Laursen.* A 3D contact smoothing method using Gregory patches. *International Journal for Numerical Methods in Engineering*, 54:1161–1194, 2002.

[13] *T. A. Laursen & J. C. Simo.* A continuum-based finite element formulation for the implicit solution of multibody, large deformation frictional contact problems. *International Journal for Numerical Methods in Engineering*, 36:3451–3485, 1993.

[14] *S. Reese, P. Wriggers & B. D. Reddy.* A new locking-free brick element technique for large deformation problems in elasticity. *Computers and Structures*, 75:291–304, 2000.

[15] *J. C. Simo, F. Armero & R. L. Taylor.* Improved versions of assumed enhanced strain tri-linear elements for 3d finite deformation problems. *Computer Methods in Applied Mechanics and Engineering*, 110:359–386, 1993.

[16] *J. C. Simo & F. Armero.* Geometrically nonlinear enhaced strain mixed methods and the method of incompatible modes. *International Journal for Numerical Methods in Engineering*, 33:1413–1449, 1992.

[17] *P. Wriggers & S. Reese.* A note on enhanced strain methods for large deformations. *Computer Methods in Applied Mechanics and Engineering*, 135:201–209, 1996.

[18] *M. A. Puso.* A highly efficient enhanced assumed strain physically stabilized hexahedral element. *International Journal for Numerical Methods in Engineering*, 49:1029–1064, 2000.

[19] *C. Beerwald, A. Brosius & M. Kleiner.* Determination of flow stress at very high strain-rates by a combination of magnetic forming and FEM calculation. *Proceeding of the International Workshop of Friction an Flow Stress in Cutting and Forming (CIRP), 25.-26.01.2000, ENSAM-Paris*.

[20] *B. Svendsen & T. Chanda.* Continuum thermodynamic formulation of models for electromagnetic thermoinelastic solids with application to electromagnetic metal forming. *in press*.

[21] *M. Badelt, C. Beerwald, A. Brosius, & M. Kleiner.* Process Analysis of Electromagnetic Sheet Metal Forming by Online-Measurement and Finite Element Simulation. *Proc. of the 6th Int. ESAFORM Conf. on Material Forming, 28.-30. April 2003, Salerno, Italy, p.123-126*.